Available online at www.sciencedirect.com

jmr&t
Journal of Materials Research and Technology

journal homepage: www.elsevier.com/locate/jmrt

Original Article

Tensile and flexural response of 3D printed solid and porous CCFRPC structures and fracture interface study using image processing technique

Nabeel Maqsood[*], *Marius Rimašauskas*

Department of Production Engineering, Faculty of Mechanical Engineering and Design, Kaunas University of Technology, 51424 Kaunas, Lithuania

ARTICLE INFO

Article history:
Received 17 April 2021
Accepted 27 June 2021
Available online 1 July 2021

Keywords:
Additive manufacturing
CCFRPC
Porous composite structure
Mechanical properties
Fracture interface imaging

ABSTRACT

Additive manufacturing is an advanced manufacturing technology that creates 3D parts geometry by depositing layers upon layers till the final part is manufactured and this technology is effectively utilized in numerous engineering applications. Due to inherently low mechanical properties of polymers, continuous carbon fiber was introduced to the thermoplastic material to form continuous carbon fiber-reinforced polymer composite (CCFRPC) to enhance their properties. This paper is going to present solid and porous CCFRPC structures manufactured by fused deposition modeling 3D printing technology. Porous composite structures were fabricated using grid infill pattern at three different infill density levels (20%, 40% and 60%) with one perimeter shell, while the solid composite specimen was fabricated with 0^{O} unidirectional layers. After the fabrication of solid and porous CCFRPC specimens, the effects on the tensile and flexural properties were experimentally examined. To study the fracture modes caused during the mechanical tests, fracture interface after performing mechanical tests was observed using microscope's micrographs which were further undergoes image processing technique to acquire edge detection (E.D), contrast enhancement (C.E) and E.D on C.E using source image (S.I) to analyze the voids and clearly identify the interface of the composite parts.

1. Introduction

3D printing, also referred to as additive manufacturing (AM), is a process of fabricating polymer, metallic, ceramic and composite parts having complex geometries layer by layer till the final product is manufactured [1,2]. The 3D part is fabricated followed by the CAD model and using the optimized printing parameters. AM technology is used for manufacturing light weight polymers and polymers matrix composite structures that have been extensively used in engineering applications such as biomedical field for tissue growth, architectural field for structural models, aerospace, construction, textile, food processing industries, automobile, electronics, military and robots etc. [3–6]. Compared to conventional and traditional manufacturing, 3D printing has the ability to shorten the

* Corresponding author.
E-mail address: nabeel.maqsood@ktu.edu (N. Maqsood).
https://doi.org/10.1016/j.jmrt.2021.06.095

design manufacturing cycle with more accuracy and perfection, thus it reduces the production cost and time [4]. Various 3D printing techniques have been industrialized for the production of polymer parts, the mainly used technologies include; Selective Laser Sintering (SLS), Stereolithography (SLA) and Fused Deposition Modelling (FDM) [2,7]. But, the pure polymer parts manufactured by these methods attains meager mechanical properties and because of their less strength and stiffness and may not be capable to be used as the purposeful components, due to lack of strength and load-bearing properties [8,9].

Different investigations have been performed and studied the poor mechanical performance of 3D printing of pure polymers and to overcome this issue. One of the possible ways is to add the reinforcement to these in the form of fibers, particles, flakes or nanomaterials to form fiber-reinforced polymer composites (FRPCs) that are viewed as elite constituents because of their outstanding performance [5]. Reinforcement used in the composite may be either continuous or discontinuous, depending on the manufacturing process [10]. However, the composite reinforced with discontinuous or short fibers has less mechanical performance compared to the composites that are reinforced with continuous fiber, and the prospect of introducing continuous FRPC will lead to much higher mechanical performance of such functional parts [11–13]. AM with improved technology that has the ability to print FRPC and resolved the limitations of poor mechanical performance of pure polymers [14]. Carbon fiber reinforced polymer composites (CFRPC) provide excellent mechanical properties. Continuous carbon fiber (CCF) has ultra-high-strength and ability to print with polymers forming continuous carbon fiber-reinforced polymer composites (CCFRPCs) [15,16]. CCFRPCs are lightweight, stiff and strong and utilized in a wide range of engineering applications. Due to exceptional mechanical properties, reusing ability and capability to be used as lightweight structures, CCFRPC are now becoming an alternative materials to substitute the traditional metals. However, in the formation of CCFRPC, the mixture of the reinforcement fibers and the polymer matrix with optimum alliance, control of fiber orientation, quantity, low cost manufacturing with the optimum mechanical performance is challenging [17,18].

Lightweight composites can be fabricated by incorporation of porous reinforcing fibrous structures that result in the reduction of the densities of composites, hence could remarkably decrease material usage, energy consumption, waste generation, and thus endorses sustainability of materials [19]. Porous structure of the part greatly depends on the infill pattern and density that also plays an important role in defining their mechanical properties [20,21]. Porous structure parts fabricated through AM have been mostly utilized in the biomedical applications in scaffold tissue and cell development as biomaterials [22,23]. The above-mentioned porous structures developed by 3D printing have mostly been applied in biomedical applications and no study is reported for structural application, especially with the CCFRPC.

FDM is the most commonly used AM technique for the production of polymers and polymer matrix composites due to ease of use, minimum wastage of material, material flexibility and low cost. This technology has the ability to print composite parts, irrespective of either continuous or discontinuous carbon fiber [24]. Most commonly used thermoplastic filaments by the FDM process include acrylonitrile butadiene styrene (ABS), polylactic acid (PLA), polypropylene (PP) or polyethylene (PE) [25]. PLA, also known as environmental-friendly polymer, one the most widely used thermoplastic, is a bio-based polymer extract from a renewable resource used to create objects using FDM 3D printers.

A. Dickson et al. [7] found the tensile strength of CCF reinforced nylon composite 6.3 times higher compared to pure nylon polymer. X. Tian et al. [7] investigated the effect of 3D printing temperatures on the composites formed by PLA with CCF and concluded that temperature ranges between 210 and 230OC shows more adequate mechanical performance. F. Ning et al. [26] studied the mechanical and microstructural properties of ABS matrix reinforced with short carbon fibers composite and achieved maximum tensile and flexural strengths of 42 MPa and 65 MPa, respectively. H.L. Tekinalp et al. [27] investigated short carbon fiber reinforced ABS composites and studied their processability, microstructure and mechanical performance. The results showed that by increasing the fiber content, voids between the printed layers decreased and the tensile strength of 3D-printed samples increased 115% compared to pure ABS. M. Rimasauskas et al. [10] prepared impregnated CCF with PLA and ABS filaments and experimental results showed that CCF reinforced PLA composite structure has the maximum tensile strength of 165 MPa. M. Heidari-Rarani et al. [28] used 1 K roving carbon fiber and prepared 3D printed CCF reinforced PLA composite by achieving highest tensile and bending strengths of 61.4 MPa and 152.1 MPa, respectively. H. Al. Abadi et al. [19] evaluated the elastic response of continuous carbon, kevlar and glass fiber reinforced with Nylon filament.

In the above reported literature, limited research has been found on illustrating the failure modes and mechanical behaviors of AM of CCFRPC [15]. Both continuous and short carbon fiber has been used with various polymers to form composite and study their mechanical performance, but no research has been performed to develop porous CCFRPC structures. This study aims to evaluate the mechanical performance of CCF reinforced PLA thermoplastic solid and porous composite structures and to compare their properties. Porous composite structure was fabricated using a grid infill pattern printed at three different infill density levels (20%, 40% and 60%). This research presents an extensive study of effects on tensile and flexural properties and comparison of solid and porous CCFRPC structures and the fracture interface was discussed after performing the mechanical testing through microscope's micrographs which were further undergoes image processing technique to acquire edge detection (E.D), contrast enhancement (C.E) and E.D on C.E using source image (S.I) to analyze the voids and clearly identify the interface of the composite parts. This technique is especially applied for the porous structure.

The present paper is prepared as follows. Firstly, the experimental methods are briefly presented, summarizing the material and specimens preparation, AM process of composite parts, experimental set-up and testing procedures. Afterward, the main results of the study are summarized, and the effects of the mechanical performance are highlighted and

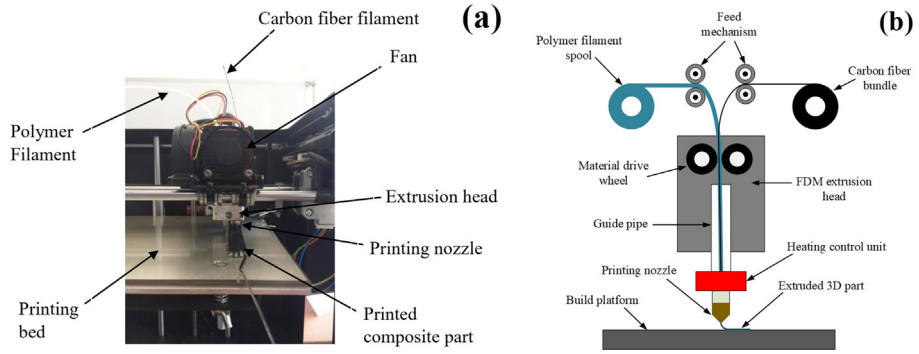

Fig. 1 – FDM 3D printing; a) equipment and printing process, b) schematic of the designed extrusion device to print CCFRPC.

discussed in detail. Finally, conclusions of this work are defined.

2. Materials, experimental set-up and measurement procedures

2.1. Materials

In this study, commercially available 3D printing PLA filament PolyLite (Polymaker) of 1.75 mm diameter was used as a matrix material having tensile strength of 46.6 MPa, Young's modulus of 2.6 GPa and density of 1.24 g/cm^3, while CCF T300B-3000 tow from Toray company was used as reinforcement material having diameter of one fiber equals to 7 μm. CCF tow (T300B) is a high-performance carbon fiber made of polyacrylonitrile having tensile strength, Young's modulus and density of 3530 MPa, 230 GPa and of 1.76 g/cm^3, respectively [29]. As, standard non-impregnated spool of CCF tow cannot be directly used for the printing. Therefore, it is necessary to impregnate standard CCF tow before the printing process. Same procedure was followed for the impregnation process of carbon fiber as discussed previously by the author [10] using the solution of PLA pellets and di-methyl chloride (CH_2Cl_2) resin for better printing quality and functioning.

2.2. Printing and process parameters

Specimen geometries for the tensile and flexural tests were modelled using the software Pro-engineer wildfire 5.0 and exported as an STL file and further imported to the 3D printing software (simplify 3D) for specimen printing preparation. MeCreator 2 (Geeetech) 3D printer was used for the manufacturing of solid and porous CCFRPC due to its simplicity and ease of use. The extrusion process of the FDM 3D printer was modified by introducing two inputs, one for PLA thermoplastic as matrix and impregnated CCF tow as reinforcement and one output where the two materials fused and extruded together. Fig. 1 shows the 3D printing equipment and schematic design of the modified extruder used for printing CCFRPC. For the printing of specimens PLA filament of 1.75 mm diameter was introduced to one input hole through a feed mechanism, while the CCF bundle was inserted to the other input directly to the printing nozzle. The drive wheel pushes both the materials towards the extrusion head to the heating unit, where the thermoplastic material melted and made a bond with the impregnated carbon fiber and they fused with each other and extruded together through the printing nozzle on the build platform.

In this study, grid infill pattern was chosen for the manufacturing of 3D printed porous composite structure with the range of infill density levels of 20%, 40% and 60% with one perimeter shell using the single tow. The perimeter shell represents the layers that deposited outside the surface prior to the filling of internal structure. The infill pattern of porous structure was covered by two upper and two bottom unidirectional layers that covered the internal structure. The internal infill angle offsets for grid pattern was printed with 45^O, -45^O. The internal layers of grid pattern deposited were counted 4 in lines. The layers were deposited using the specified path defined by the Simplify 3D. While, for the 100% infill composite specimen, unidirectional 0° flat specimen was selected to print for the experiment and isotropic fiber pattern was analyzed in this case without any perimeter shell. Fig. 2 shows the infill patterns of 3D printed specimens fabricated for this experimental study. Printing parameters are presented in Table 1.

2.3. Tensile and flexural testing

Tensile and flexural properties of 3D printed CCFRPC were carried out to study and analyze the performance of composite parts. In the present research, ASTM D3039 [30] standard was used to perform tensile, while D790 [31] standard was used to perform flexural test of the specimens. According to the mentioned tensile and flexural testing standards, five specimens were prepared to determine their properties and a total 40 specimens were printed for the testing.

As there is no specified geometry is defined for the CCFRPC parts fabricated using FDM technology. Therefore, for the tensile test, the specimens having dimensions 150 × 13 × 3 mm of rectangular cross-section were fabricated and weighted before applying the tabs. For the grip PLA tabs having dimensions 50 × 12.5 × 2 mm with the bevel angle of 30^O were applied on each tensile test specimen. Four points were marked 15 mm from the center of the specimens in order

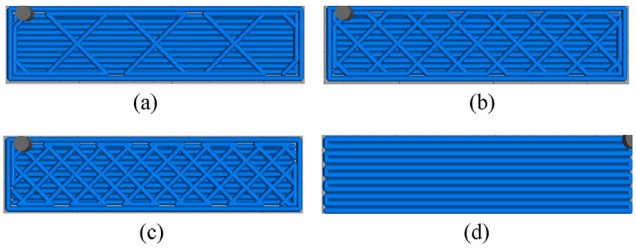

Fig. 2 – Infill patterns of 3D printed specimens fabricated with Grid infill a) 20%, b) 40%, c) 60% and unidirectional with infill d) 100%.

to measure the elastic strain. The test was performed using the standard head displacement rate of 2 mm/min.

For the three-point bending flexural test, rectangular cross-section specimens having dimensions 127 × 12.7 × 3.2 mm were fabricated. The test was performed using the crosshead motion rate and span support length of 1.35 mm/min and of 51.2 mm, respectively. Tinius Olsen H25KT (capacity 25 kN) universal testing machine was used to perform both the tests, as it has the ability to convert to dual column as well as three-point bending set-up. Dimensions of 3D printed specimens are presented in Table 2.

2.4. *Fracture interface study of the specimens*

Fracture interface study was performed on the specimens after performing tensile and flexural tests and observed using microscope (Delta Optical Smart) micrographs. This experiment was performed to study the failure mode and response of the deposited layers and detached and the ruptured fibers in the matrix after performing the mechanical tests. The obtained images from microscope were further undergone image processing technique to enhance the quality of the source image for detailed study.

2.4.1. *Contrast enhancement*

This image processing technique is used to enhance the image having poor contrast. The histogram equalization seems an effective technique to improve the contrast of an image. In this regard, Non-Parametric Modified Histogram Equalization (NPMHE) [32,33] is utilized to improve the contrast of an image and preserve the low brightness of the source image A_i.

$$X_i \rightarrow X_i' \tag{1}$$

NPMHE is employed to fracture interface images to obtain an improved image X_i'. Contrast enhancement centrally improves the intensity distribution and enhances the image details.

2.4.2. *Edge detection*

After performing contrast enhancement, the images are then rectified through spatial stimuli sketch model (SSGSM) [34,35] based edge detection technique to acquires the object boundaries through detection of brightness discontinuities [36]. Edge detection improves performance when used on high

Table 1 – 3D printing parameters used for CCFRPC specimens.

Nozzle diameter	1.5 mm
Extrusion multiplier	0.5
Extrusion width	1.5 mm
Layer height	0.5 mm
Printing speed	3.0 mm/s
Extruder temperature	210^{O}C
Bed temperature	90^{O}C
Fan speed	60%

contrast images. This method emphases on the intensity of the focus and the edges of the image and calculates an unknown area on the coarse solution map to achieve information that is focused on the two activity level maps. The weight of the local stimuli is intentionally adjusted by determining the local change in brightness perceived at each site. The brightness of the contrast enhanced image X_i' is perceived in Eq. (2) as:

$$E_i = z log_{10}(X_i') \tag{2}$$

where, X_i' represents the contrast enhanced image and denotes the scaling factor. Gradients indicate strong changes in image intensity.

It is a measure of spatial distance to the measured variation of local pixels. This amplitude is mathematically computed as the mesh difference in identified brightness in *r* and *s* directions as:

$$B_i = gradient\left[\sigma_j^r,\ \sigma_j^s\right] \tag{3}$$

$$\zeta_j^r = \sigma_j^r\left(e^{-\left|\sigma_j^r\right|}\right); \zeta_j^s = \sigma_j^s\left(e^{-\left|\sigma_j^s\right|}\right) \tag{4}$$

where, intensity variations (B_i) on the *r* and *s* axis denoted by ζ_j^r and ζ_j^s respectively. These variations are computed in Eq. (3) and Eq. (4) by employing the corresponding gradients σ_j^r, σ_j^s.

The local stimuli (L_i) is calculated in Eq. (5) as:

$$L_i = \sqrt{\left(\zeta_j^r\right)^2 + \left(\zeta_j^s\right)^2} \tag{5}$$

3. Experimental results and discussions

3.1. *Observation of printing process parameters and specimen geometry*

The porous specimens were fabricated using a grid infill pattern that represents the internal geometry structure of the composite part at three different infill density levels (20%, 40% and 60%). The infill structure was covered within one perimeter shell and with two bottom and two top unidirectional layers as shown in Fig. 2. By increasing the infill density, the internal structure of the specimen increases by addition of unit cells to the porous structure, while the outer wall layer remains the same. Irregular distribution of the layers were observed during the printing process. This is due to the infill paths created by the simplify 3D that is also an important

Table 2 – Dimensions of 3D printed specimens.

Infill	Tensile specimen				Flexural specimen			
	Length, mm	Width, mm	Thickness, mm	Mass, g	Length, mm	Width, mm	Thickness, mm	Mass, g
20%	150.68 ± 0.47	13.08 ± 0.13	3.08 ± 0.05	6.05 ± 0.05	126.33 ± 0.74	12.73 ± 0.08	3.31 ± 0.08	3.86 ± 0.05
40%	150.86 ± 0.39	13.07 ± 0.08	3.11 ± 0.06	6.58 ± 0.07	126.25 ± 0.27	12.78 ± 0.04	3.27 ± 0.03	4.09 ± 0.06
60%	150.64 ± 0.62	13.04 ± 0.03	3.09 ± 0.06	7.05 ± 0.09	126.83 ± 0.03	12.77 ± 0.07	3.23 ± 0.02	4.28 ± 0.04
100%	150.78 ± 0.56	13.08 ± 0.11	3.06 ± 0.07	7.89 ± 0.06	126.95 ± 0.04	12.73 ± 0.05	3.25 ± 0.04	5.27 ± 0.06

feature of anisotropy [37]. The grid infill structure has a nodal connectivity equal to 4 which is known to be anisotropic [38,39]. The specimen with 100% infill density level was printed with 0^{O} unidirectional layers without any perimeter shell.

Fig. 3 (a and b) represents the mass as a function of infill percentage for the 3D printed specimens fabricated for tensile and flexural tests. The mass of each specimen with the increase in infill density level increases. Increasing the infill percentage will lead to occupying more space compactly within the shell, since the perimeter shell, bottom and top layers remain the same. Significant increase in the mass can be observed when the infill density level rises from 60% to 100%. The mass in case of tensile test specimens can be seen higher due to higher in length compared to flexural test specimens. The internal structure and pattern defined within the specimen geometry define the mechanical properties [38] of the composite part.

3.2. *Tensile test response of composite parts*

Effects on tensile properties (tensile strength, young's modulus and ductility) were studied and compared by performing tensile tests of each group of specimens. Typical tensile stress–strain curves of each set of groups are presented in Fig. 4. Selection of the curves were made according to the mean results i.e. the curve that showed average tensile strength are presented and marked up to the point of breakage.

It can be observed from the stress–strain curves that the specimen printed with 100% infill density level achieved the largest level of strength, while the specimen printed with 20% infill density level showed minimum tensile strength. 40% and 60% infill density specimens were marked at average level between them. The tensile properties of each set of groups are shown in Fig. 5. Box plots were used to represent the effect of tensile properties obtained from the tensile test, showing the average values with the range of maximum and minimum standard deviation values of the 3D printed composite parts.

According to ASTM D3039 [30], 3D printed composite specimens showed Lateral-at tab-top (LAT) and edge delamination-gage- middle (DGM) failure modes. The difference in the failure modes is caused due to various condition circumstances under the same test conditions that includes gripping pressure, specimen geometry and tab material of the specimens [40]. The outcomes of tensile properties estimated from the tensile test is illustrated in Table 3.

3.2.1. *Tensile strength*

The tensile strength of the CCFRPC specimens of each infill density level is shown in Fig. 5(a). From the box plot, it can be observed that the specimen fabricated with 100% infill density reaches the largest mean tensile strength of 253.25 MPa While, the composite specimens with 20%, 40% and 60% infill density levels showed average tensile strength values of 150.16 MPa, 165.32 MPa and 171.48 MPa, respectively. 100% infill density level specimen's tensile strength increased by 68%, 53% and 48% compared to 20%, 40% and 60% infill density levels specimens, respectively, which showed a dramatic increase in the strength value. The result indicated that, by increasing the infill density level, strength will increase. Maximum tensile strengths of the PLA printed with CCF composite parts with 100% infill achieved were 91 MPa, 61.4 MPa and 170 MPa [10,28,41]. Compared to previously obtained results, porous composite parts showed significant

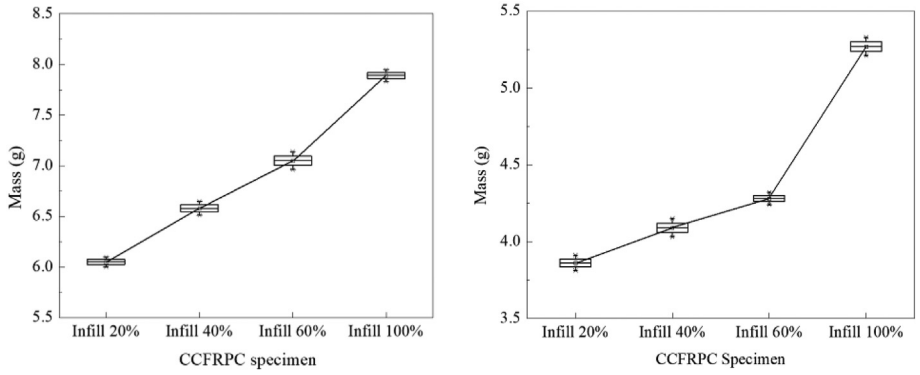

(a) Tensile test (b) Flexural test

Fig. 3 – CCFRPC specimens mass as a function of infill percentage.

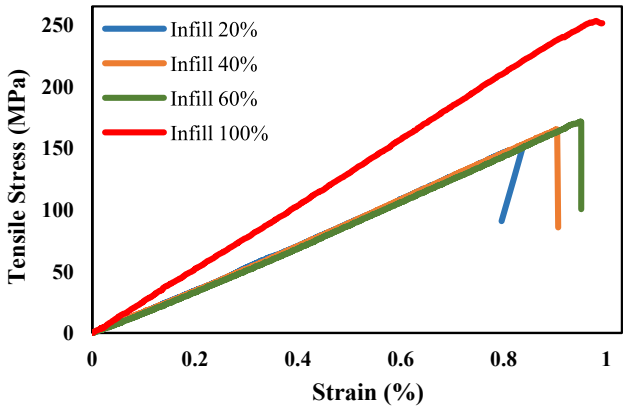

Fig. 4 – Stress–strain curve obtained from the tensile test.

comparison in the tensile strength result that have been almost reached to the same level even contrast to 20% infill density level specimen.

3.2.2. *Young's modulus*

The young's modulus of the 3D printed composite parts of each infill density level is shown in Fig. 5(b). The largest young's modulus value of 25.75 GPa can be seen in the composite specimen with 100% infill density. The specimen with 20% infill density showed the lowest young's modulus value by reaching 16.61 GPa. While the 40% and 60% infill density levels specimens showed average young's modulus values of 17.53 GPa and 18.24 GPa, respectively. Significant increase in the Young's modulus value can be observed when the infill density was increased from 60% to 100% infill density. The result indicated that by increasing the infill density, carbon fiber content in the matrix increases that lead to increase in the young's modulus value [13,26].

3.2.3. *Ductility*

The Ductility of the 3D printed composite specimens of each infill density level is shown in Fig. 5(c). From the figure, it can be observed that the CCFRPC part with 20% infill had the smallest average ductility of 2.62%, while the largest mean ductility value of 3.3% can be seen in specimens with 100% infill density level. The result confirms the increase in the ductility with the increase in infill density level of the composite part.

3.3. *Flexural test response of composite parts*

Effects on flexural properties (flexural stress and flexural modulus) of the 3D printed solid and porous CCFRPC specimens were obtained and studied by performing flexural test

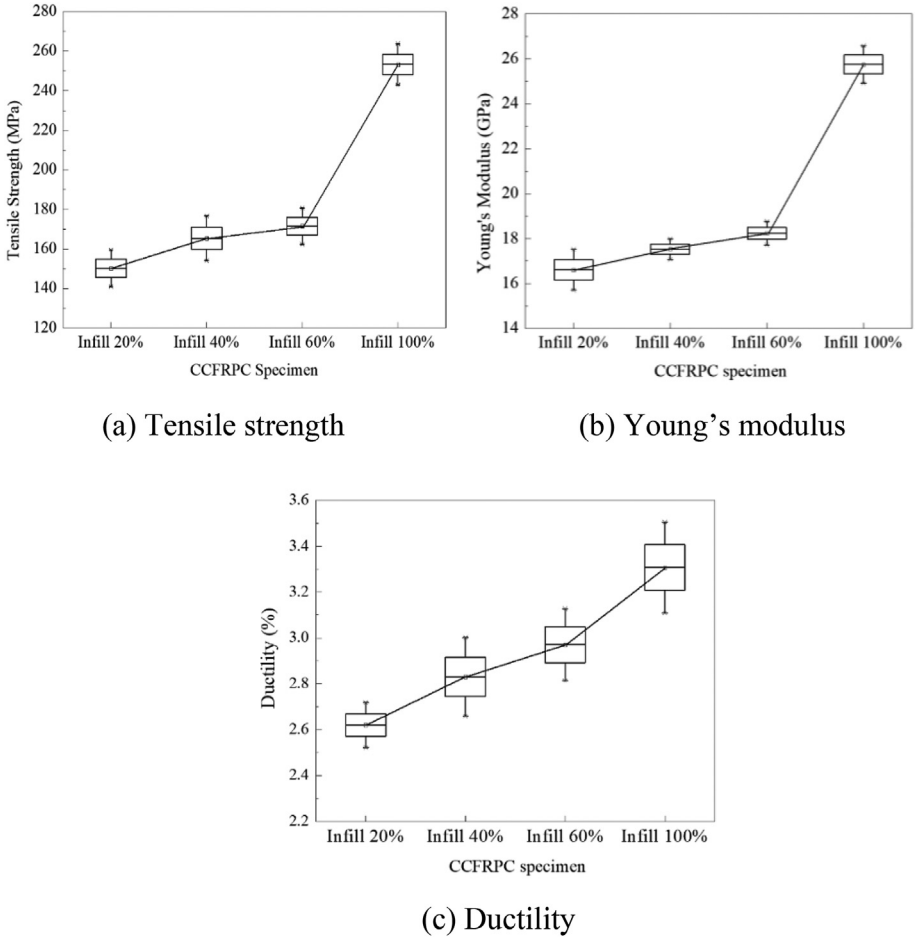

Fig. 5 – Results of tensile properties obtained from the tensile test.

Table 3 – Results of mechanical properties measured.

Specimens	Tensile Properties			Flexural Properties	
	Tensile strength (MPa)	Young's modulus (GPa)	Ductility (%)	Flexural strength (MPa)	Flexural modulus (GPa)
Infill 20%	150.16 ± 9.27	16.61 ± 0.91	2.62 ± 0.1	105.99 ± 9.51	10.82 ± 1.52
Infill 40%	165.32 ± 11.26	17.53 ± 0.46	2.83 ± 0.17	115.89 ± 8.55	11.02 ± 1.04
Infill 60%	171.48 ± 9.14	18.24 ± 0.53	2.97 ± 0.15	130.1 ± 8.68	12.18 ± 0.89
Infill 100%	253.25 ± 10.42	25.75 ± 0.83	3.3 ± 0.19	173.48 ± 9.85	14.77 ± 1.45

for each set of groups. Referring to the ASTM D790 standard [31], flexural tests would be valid, if the maximum strain of the specimen breakage in the outer region occurred within the 5% strain limit. During the test, 3D printed CCFRPC specimens rupture in the outer region occurred within the 5% strain limit. Typical flexural stress–strain curves of each infill density level are demonstrated in Fig. 6. Selection of the stress–strain curve results presented in the figure were made that represent average flexural strength levels of each set of groups.

From the stress–strain curves, it can be perceived that the composite specimen with 100% infill showed maximum flexural stress level. Similarly, decreasing the infill density level tends to decrease in the flexural stress value. The flexural properties of CCFRPC parts are shown in Fig. 7. Box plots were used to illustrate the flexural properties, showing the average values with the range of maximum and minimum standard deviation values of the 3D printed composite parts result effects on the flexural properties.

3.3.1. *Flexural strength*

The flexural strength of the 3D printed solid and porous CCFRPC parts of each infill density level is presented in Fig. 7(a). From the box plot graph, the specimen fabricated with 100% infill density had the largest flexural strength value of 173.48 MPa. While, the composite specimens fabricated with 20%, 40% and 60% infill density levels had average flexural strength values of 105.99 MPa, 115.89 MPa and 130.1 MPa, respectively. Increasing the infill density level leads to increase in flexural strength. CCF reinforced PLA composite specimens printed with 100% infill density level showed highest flexural strength, increased by 63.6%, 49.7% and 33.3%, respectively, compared to 20%, 40% and 60% infill density levels of composite specimens. The same result can also be observed [15], that showed the increase in the flexural strength values by increasing the content of carbon fiber in the composite.

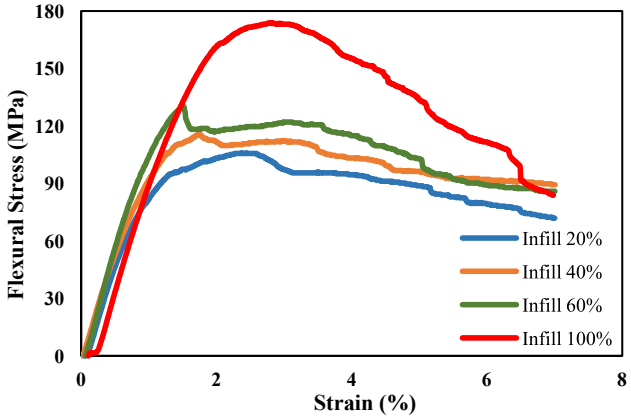

Fig. 6 – Stress–strain curve obtained from the flexural test.

3.3.2. *Flexural modulus*

The flexural modulus of the composite specimens prepared with the range of infill density levels are presented in Fig. 7(b). The largest flexural modulus value of 14.77 GPa can be seen in the 100% infill density level CCFRPC specimen. Composite specimens printed with 20%, 40% and 60% infill density levels had mean flexural modulus values of 10.82 GPa, 11.02 GPa and 12.18 GPa, respectively. The results indicated that by increasing the infill density of the structure increases the flexural modulus of the CCFRPC part.

3.4. *Study of fracture interface after mechanical testing*

To observe the deformation and fracture behavior that how the fracture occurred during the mechanical test, fracture interface of the CCFRPC solid and porous composite fractured specimens was decided to study based on the experimental results of tensile and flexural tests. To study such behavior, microscope's micrographs were carried out after performing tensile and flexural tests. For this purpose, one specimen of each infill density was selected that reflects the best failure mode. Microscope's micrographs were carried out at 1.5 mm of scale and this scale was kept constant for all the images of each specimen. The obtained micrographs further undergoes image processing technique to acquire E.D using S.I. The S.I is subjected further to get C.E images, which were further processed to achieve E.D on C.E image to analyze the voids and clearly study the fracture interface modes of the composite parts.

Fracture interface's micrographs E.D, C.E and E.D on C.E using S.I of the specimen after performing tensile tests are shown in Fig. 8. From the figure, it can be observed that the matrix layers were separated from each other holding the impregnated CCF within it after the tensile test was performed. The fracture occurred at the maximum load during the experiment. Fig. 8 (a-c) showed the micrographs of porous composite parts. The gaps and more voids area can be seen in case of porous specimens, the reason is due to hollow structure inside, while the perimeter shell is visible. More cavities are clearly visible at low infill density specimens. Further increasing the infill density level decreases the gaps and hollow structure inside the specimen. The major reason for the fracture of such a structure is caused due to fiber pull out [13,41,42]. The CCF stills hold the matrix within it at various

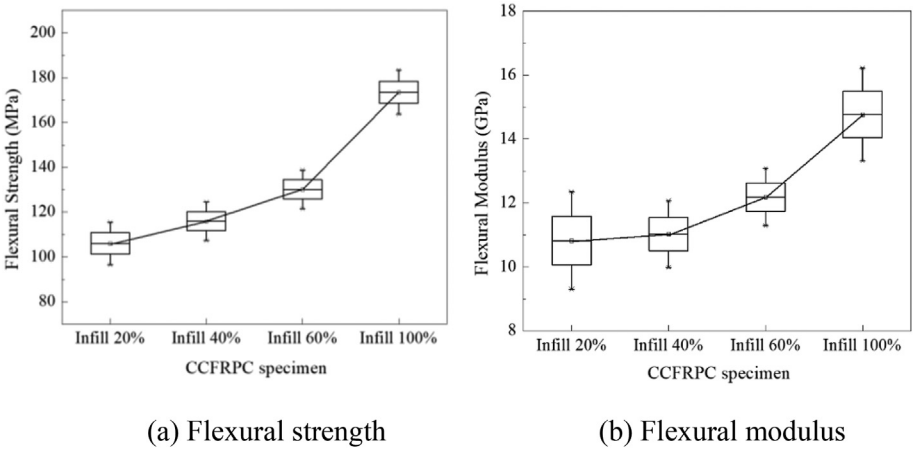

(a) Flexural strength (b) Flexural modulus

Fig. 7 – Results of flexural properties obtained from the flexural test.

portions and resulted in it could be used for load bearing and structural applications during tension, as load was effectively shifted from matrix to fiber.

Fig. 9 shows the fracture interface's micrographs E.D, C.E and E.D on C.E using S.I of the specimen after performing flexural test. A fractured region is clearly visible, where the breakage occurred upon bending force. Matrix layers were separated instantly, letting the reinforcement material behind it. In case of 100% infill density level specimens, more dense structure can be observed compared to porous structures,

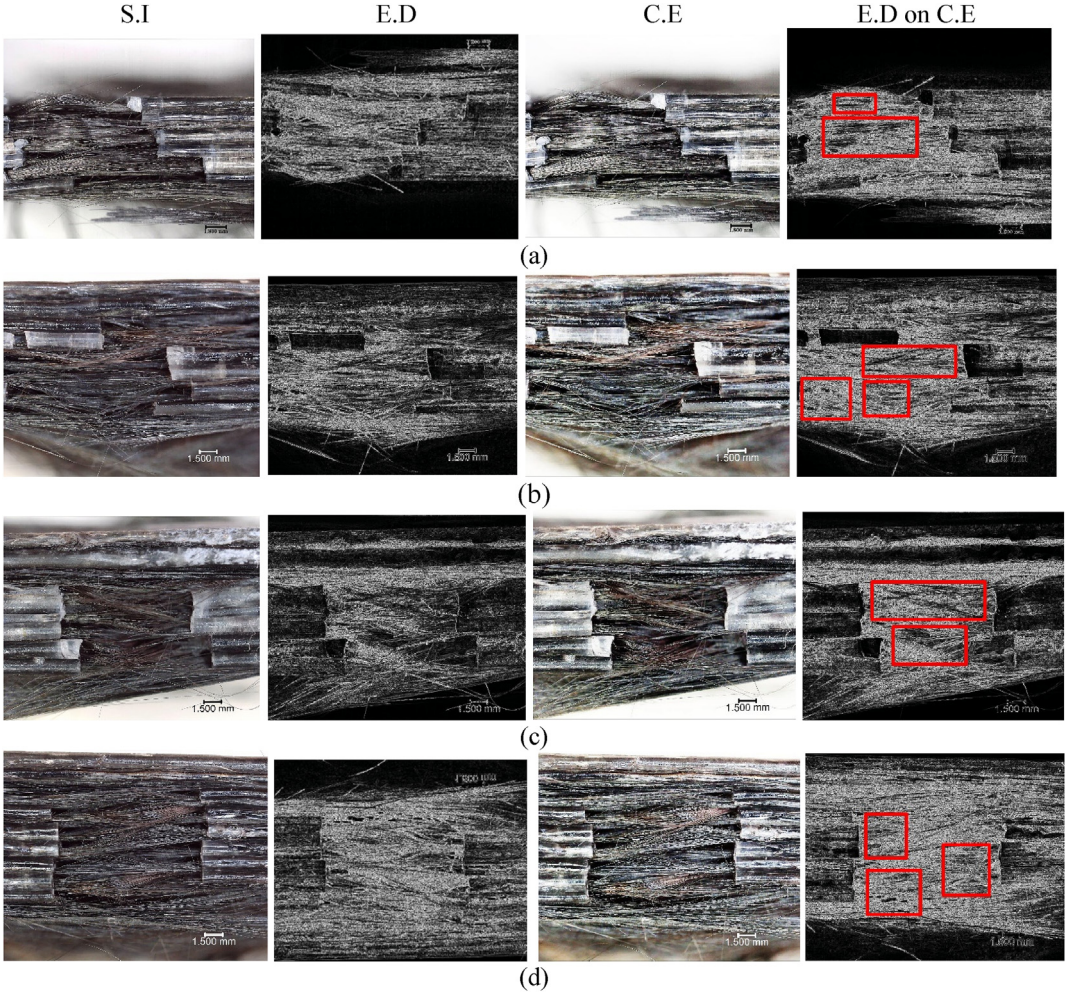

Fig. 8 – Fracture interface's micrographs E.D, C.E and E.D on C.E using S.I of the specimen after performing tensile test with infill density level of (a) 20% (b) 40% (c) 60% (d) 100%.

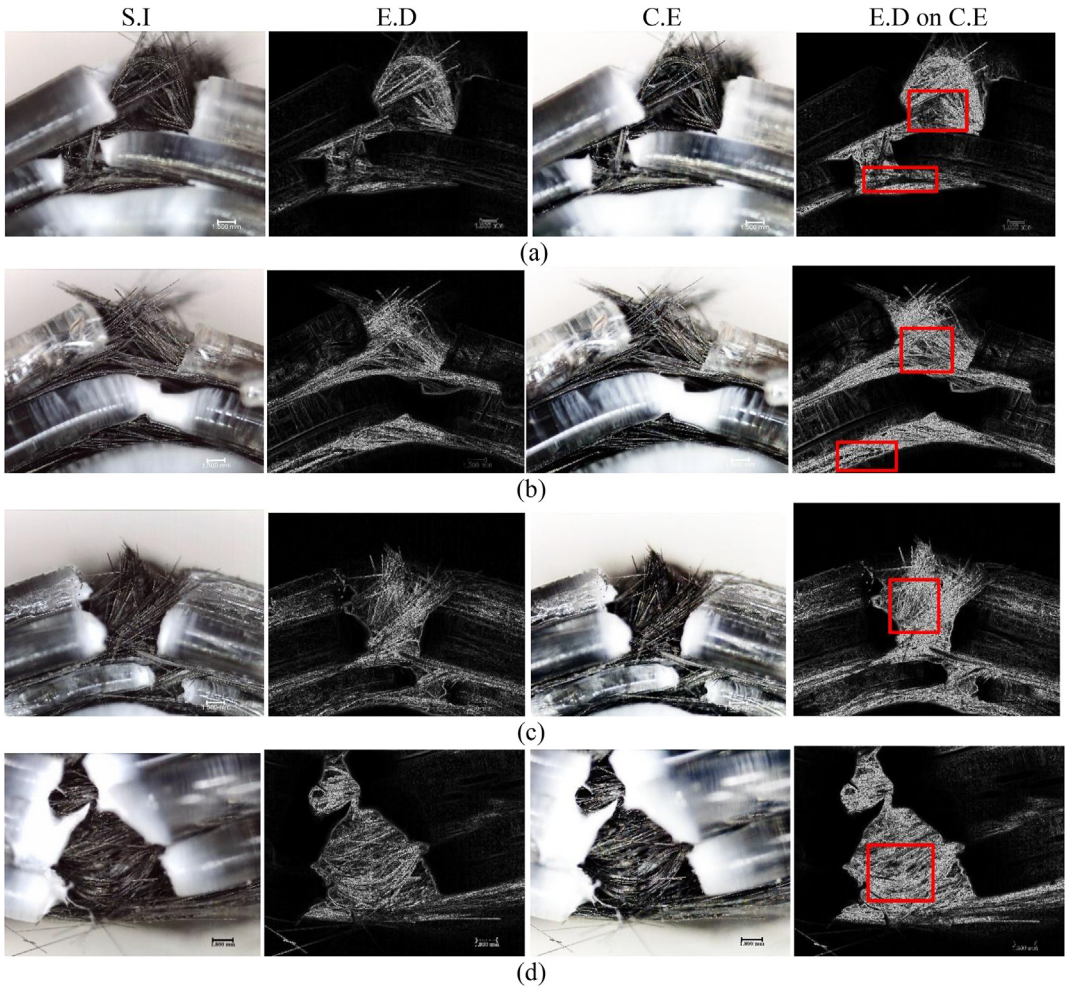

Fig. 9 – Fracture interface's micrographs E.D, C.E and E.D on C.E using S.I of the specimen after performing flexural test with infill density level of (a) 20% (b) 40% (c) 60% (d) 100%.

while the voids and hollow region is noticeable in case of porous structure. This reason can also be enlightened and validated by attaining the highest flexural stress level among the group. Increasing infill density level resulted in a more dense structure with low level of porosity inside the specimen shell. The CCF upon bending test separated from the matrix material layers at various instant. However, this is caused due to broken carbon fibers. The main reason for the dominant failure mode of the CCFRPC structure was mainly broken fibers [26,43].

3.5. *Effects of continuous carbon fiber content*

The specimens with three infill density levels had different content of reinforcement. It varies with the specimen's size, geometry, extrusion multiplier, infill pattern and density. The carbon fiber content was estimated using the length of tool path, number of layers in length and width of the specimen. Therefore, the CCF content measured can be considered as the weight ratio of carbon fiber content to the matrix material. Although the number of layers in porous structures were the same but occupied less portion inside the shell and most of the portion was hollow. Increasing the infill density level, the structure inside the shell was occupied more compactly, forming a more dense structure and more material was consumed. Increasing the material quantity will result in an increase in reinforcement content. For each case, the increasing infill density of the composite part resulted in an increase in CCF content.

Table 4 shows the carbon fiber contents of CCFRPC parts with different infill density levels. The results showed that increasing the infill density level of CCFRPC specimen lead to increase in carbon fiber content and each set of specimen with increased infill density showed high tensile strength and flexural stress as shown in Fig. 5(a) and 7(a), respectively. Hence, it was demonstrated that by increasing the CCF content, the strength of the composite part increased. This result is also validated by the previous achieved results [41,44]. This study estimated the synergistic reinforcement of CCF for porous composite parts printed with the infill ranges of 20%, 40% and 60%, CCFRPC specimens were prepared with geometry dimensions of 3.6 cm^3. The total numbers of layers in

Table 4 – Carbon fiber contents of CCFRPC specimens with different infill density levels.

Specimens	Volume of CCFRPC specimens (cm^3)	CCF content volume fraction (vol. %)	CCF content weight fraction (wt.%)
Infill 20%	3.63	8.91	12.2
Infill 40%	3.67	10.9	14.8
Infill 60%	3.62	12.84	17.3

Volume fraction of fiber (V_f) is listed in Table 4, E_f is equals to 230 GPa and E_m is given by 2.6 GPa. Applying this technique to the composite parts with different volume fractions allowed us to estimate the elastic modulus of composite parts. The estimated elastic modulus of porous composite structures with 20%, 40% and 60% infill density levels were 20.3 GPa, 24.8 GPa and 29.2 GPa, respectively which showed highest elastic modulus value that can also be validated by the tensile test outcome. Rule of mixture estimated the maximum optimum elastic modulus for the designed composite parts

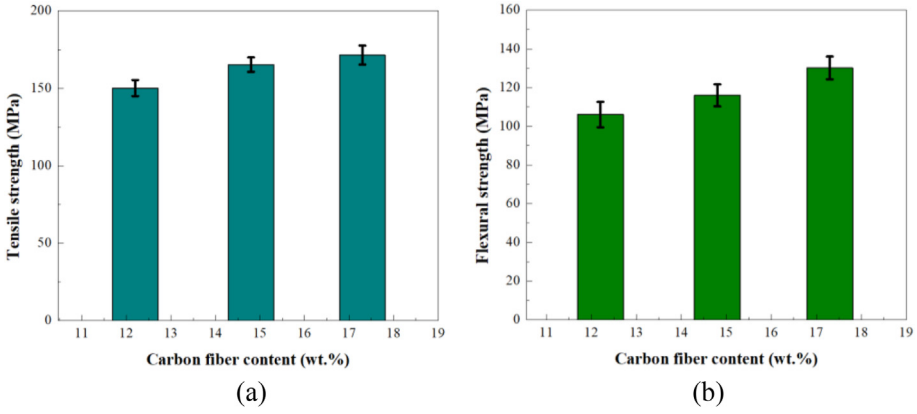

Fig. 10 – Effect of carbon fiber content on a) Tensile strength and b) Flexural strength.

length and width calculated were 6 and 7, respectively. CCF volume fractions V_f was obtained from the weight fraction W_f using the following formula [44].

$$V_f = \frac{W_f}{W_f + \frac{\rho_f}{\rho_m}(1 - W_f)} \quad (6)$$

where, V_f is the volume fractions of carbon fiber, W_f is the weight fraction of the carbon fiber of each specimen, ρ_f is the density of CCF (1.76 g/cm^3) and ρ_m is the density of PLA matrix (1.24 g/cm^3). Fig. 10 shows the effect of carbon fiber content on the tensile strength and flexural stress of the composite parts.

3.6. *Rule of mixtures*

The theoretical tensile strength and elastic modulus could be assessed based on the mechanical properties of the carbon fiber and composite parts obtained in section 3 (Table 3) of the solid and porous CCFRPC parts manufactured via FDM 3D printing method. In this study, the elastic modulus of prepared composite solid and porous parts was estimated using Eq. (7), as the fibers are printed parallel to the matrix in each case.

$$E_c = V_f.E_f + (1 - V_f).E_m \quad (7)$$

where, E_c = elastic modulus of composite, V_f = volume fraction of fiber, E_f = elastic modulus of fiber, E_m = elastic modulus of matrix.

demonstrated that the CCFRPC parts possessed high elastic modulus. Increasing the content of CCF, both theoretical and experimental values of modulus increases and this could result in the decrease in porosity [27].

4. Conclusion

In this study solid and porous CCFRPC specimens were prepared using FDM 3D printing technology. Porous composite structures were fabricated using grid infill pattern printed at three different infill density levels (20%, 40% and 60%). Effects on tensile and flexural properties were experimentally investigated and compared. Afterwards, fracture interfaces of the 3D printed CCFRPC specimens were observed and analyzed using a microscope's micrographs after performing mechanical tests. Following conclusions were drawn from this study.

1. Porous composite specimens with grid infill pattern showed increase in tensile strength and Young's modulus with the increase in infill percentage by achieving highest strength and modulus values of 171.48 MPa and 18.24 GPa, respectively in 60% infill density level.
2. Highest flexural strength and modulus values of 130.1 MPa and 12.18 GPa, respectively were found in 60% infill density level among the porous grid infill pattern structures. The result also indicated that increasing infill density level leads to increase in flexural strength and modulus.

3. Enhanced fracture interface's micrographs through image processing technique of the composite specimens after performing mechanical tests showed that the dominant failure mode of such structure was caused due to fiber breakage and pull out. The fiber still holds the matrix within it at various portions of the interfacial layers. Hence, the result was that it could be used for load bearing applications.
4. Effect of carbon fiber content on mechanical properties showed the increase in tensile strength and flexural strength value with the increase in the fiber content.
5. The porous structure presented in this study exhibited great potential to be utilized in structural engineering applications as it showed enhanced strength levels compared to previously achieved strengths and it could probably have ability to replace fully dense or solid structure, as it consumes less material, mass and carbon fiber content.

Declaration of Competing Interest

The authors declare that they have no known competing interests or personal relationships that could have appeared to influence the work reported in this paper.

Acknowledgment

The authors are thankful to Mr. Sarmad Maqsood, Department of Software Engineering, Faculty of Informatics Engineering, Kaunas University of Technology for helping us in acquiring the results of fracture interface through imaging processing technique and his assistance in the software.

REFERENCES

[1] ASTM International. ASTM F2792-12a. Rapid manufacturing association. 2013. p. 1–3. https://doi.org/10.1520/F2792-12A.2.
[2] Maqsood N, Rimasauskas M. A review on development and manufacturing of polymer matrix composites using 3D printing technologies. In: 9th international scientific conference on defensive technologies. OTEH; 2020. p. 462–8.
[3] El Moumen A, Tarfaoui M, Lafdi K. Additive manufacturing of polymer composites: processing and modeling approaches. Compos B Eng 2019;171:166–82. https://doi.org/10.1016/j.compositesb.2019.04.029.
[4] Parandoush P, Lin D. A review on additive manufacturing of polymer-fiber composites. Compos Struct 2017;182:36–53. https://doi.org/10.1016/j.compstruct.2017.08.088.
[5] Wang X, Jiang M, Zhou Z, Gou J, Hui D. 3D printing of polymer matrix composites: a review and prospective. Compos B Eng 2017;110:442–58. https://doi.org/10.1016/j.compositesb.2016.11.034.
[6] Karayel E, Bozkurt Y. Additive manufacturing method and different welding applications. Journal of Materials Research and Technology 2020;9:11424–38. https://doi.org/10.1016/j.jmrt.2020.08.039.
[7] Dickson AN, Barry JN, McDonnell KA, Dowling DP. Fabrication of continuous carbon, glass and Kevlar fibre reinforced polymer composites using additive manufacturing. Additive Manufacturing 2017;16:146–52. https://doi.org/10.1016/j.addma.2017.06.004.
[8] Akram W, Rafique AF, Maqsood N, Khan A, Badshah S, Khan RU. Characterization of PTFE film on 316L stainless steel deposited through spin coating and its anticorrosion performance in multi acidic mediums. Materials 2020;13. https://doi.org/10.3390/ma13020388.
[9] Nebe M, Schmack T, Schaefer T, Walther F. Composites Part C: open Access Experimental and numerical investigation on the impact response of CFRP under 3-point-bending. Composites Part C: Open Access 2021;4:100079. https://doi.org/10.1016/j.jcomc.2020.100079.
[10] Rimašauskas M, Kuncius T, Rimašauskienė R. Processing of carbon fiber for 3D printed continuous composite structures. Mater Manuf Process 2019;34:1528–36. https://doi.org/10.1080/10426914.2019.1655152.
[11] Ivanova O, Williams C, Campbell T. Additive manufacturing (AM) and nanotechnology: promises and challenges. Rapid Prototyp J 2013;19:353–64. https://doi.org/10.1108/RPJ-12-2011-0127.
[12] Chakraborty S, Biswas MC. 3D printing technology of polymer-fiber composites in textile and fashion industry: a potential roadmap of concept to consumer. Compos Struct 2020;248:112562. https://doi.org/10.1016/j.compstruct.2020.112562.
[13] Maqsood N, Rimašauskas M. Characterization of carbon fiber reinforced PLA composites manufactured by fused deposition modeling. Composites Part C: Open Access 2021;4:100112. https://doi.org/10.1016/j.jcomc.2021.100112.
[14] Dong C. Flexural behaviour of carbon and glass reinforced hybrid composite pipes. Composites Part C: Open Access 2021;4:100090. https://doi.org/10.1016/j.jcomc.2020.100090.
[15] Yu T, Zhang Z, Song S, Bai Y, Wu D. Tensile and flexural behaviors of additively manufactured continuous carbon fiber-reinforced polymer composites. Compos Struct 2019;225:111147. https://doi.org/10.1016/j.compstruct.2019.111147.
[16] Zappino E, Filippi M, Pagani A, Petiti M, Carrera E. Experimental and numerical analysis of 3D printed open-hole plates reinforced with carbon fibers. Composites Part C: Open Access 2020;2:100007. https://doi.org/10.1016/j.jcomc.2020.100007.
[17] Bettini P, Alitta G, Sala G, Di Landro L. Fused deposition technique for continuous fiber reinforced thermoplastic. J Mater Eng Perform 2017;26:843–8. https://doi.org/10.1007/s11665-016-2459-8.
[18] Mouritz Adrian P. Introduction to aerospace materials. 1st ed. Cambridge, England: Woodhead Publishing Ltd; 2012.
[19] Al Abadi H, Thai HT, Paton-Cole V, Patel VI. Elastic properties of 3D printed fibre-reinforced structures. Compos Struct 2018;193:8–18. https://doi.org/10.1016/j.compstruct.2018.03.051.
[20] Sharma R, Singh R, Penna R, Fraternali F. Investigations for mechanical properties of Hap, PVC and PP based 3D porous structures obtained through biocompatible FDM filaments. Compos B Eng 2018;132:237–43. https://doi.org/10.1016/j.compositesb.2017.08.021.
[21] Ang KC, Leong KF, Chua CK, Chandrasekaran M. Investigation of the mechanical properties and porosity relationships in fused deposition modelling-fabricated porous structures. Rapid Prototyp J 2006;12:100–5. https://doi.org/10.1108/13552540610652447.
[22] Bose S, Ke D, Sahasrabudhe H, Bandyopadhyay A. Additive manufacturing of biomaterials. Prog Mater Sci 2018;93:45–111. https://doi.org/10.1016/j.pmatsci.2017.08.003.

[23] Maqsood N, Khan A, Alamgir MK, Shah SA, Fahad M. PTFE thin film coating on 316L stainless steel for corrosion protection in acidic environment. J Eng Appl Sci 2017;36:183–90.
[24] Justo J, Távara L, García-Guzmán L, París F. Characterization of 3D printed long fibre reinforced composites. Compos Struct 2018;185:537–48. https://doi.org/10.1016/j.compstruct.2017.11.052.
[25] Horn TJ, Harrysson OLA. Overview of current additive manufacturing technologies and selected applications. Sci Prog 2012;95:255–82. https://doi.org/10.3184/003685012X13420984463047.
[26] Ning F, Cong W, Qiu J, Wei J, Wang S. Additive manufacturing of carbon fiber reinforced thermoplastic composites using fused deposition modeling. Compos B Eng 2015;80:369–78. https://doi.org/10.1016/j.compositesb.2015.06.013.
[27] Tekinalp HL, Kunc V, Velez-Garcia GM, Duty CE, Love LJ, Naskar AK, et al. Highly oriented carbon fiber-polymer composites via additive manufacturing. Compos Sci Technol 2014;105:144–50. https://doi.org/10.1016/j.compscitech.2014.10.009.
[28] Heidari-Rarani M, Rafiee-Afarani M, Zahedi AM. Mechanical characterization of FDM 3D printing of continuous carbon fiber reinforced PLA composites. Compos B Eng 2019;175:107147. https://doi.org/10.1016/j.compositesb.2019.107147.
[29] Toray Composite Materials America. T300 standard modulus carbon fibers. 2018. https://doi.org/10.2115/fiber.66.p_184.
[30] ASTM. Standard test method for tensile properties of polymer matrix composite materials ASTM D3039/D3039M. Annual Book of ASTM Standards; 2014. p. 1–13. https://doi.org/10.1520/D3039.
[31] American Society for Testing and Materials. Standard test methods for flexural properties of un-reinforced and reinforced plastics and electrical insulating materials, D790M-86. Annual Book of ASTM Standards,0801, Plastics (1), C177-D1600 1989;i:290–8. https://doi.org/10.1520/D0790-17.
[32] Maqsood S, Javed U. Multi-modal medical image fusion based on two-scale image decomposition and sparse representation. Biomed Signal Process Contr 2020;57:101810. https://doi.org/10.1016/j.bspc.2019.101810.
[33] Poddar S, Tewary S, Sharma D, Karar V, Ghosh A, Pal SK. Non-parametric modified histogram equalisation for contrast enhancement. IET Image Process 2013;7:641–52. https://doi.org/10.1049/iet-ipr.2012.0507.
[34] Mathew JJ, James AP. Spatial stimuli gradient sketch model. IEEE Signal Process Lett 2015;22:1336–9. https://doi.org/10.1109/LSP.2015.2404827.
[35] Maqsood S, Damaševičius R, Maskeliūnas R. Hemorrhage detection based on 3D CNN deep learning framework and feature fusion for evaluating retinal abnormality in diabetic patients. Sensors 2021;21:3865. https://doi.org/10.3390/s21113865.
[36] Muzammil SR, Maqsood S, Haider S, Damaševičius R. CSID: a novel multimodal image fusion algorithm for enhanced clinical diagnosis. Diagnostics 2020;10:904. https://doi.org/10.3390/diagnostics10110904.
[37] Clausen A, Aage N, Sigmund O. Exploiting additive manufacturing infill in topology optimization for improved buckling load. Engineering 2016;2:250–7. https://doi.org/10.1016/J.ENG.2016.02.006.
[38] Lubombo C, Huneault MA. Effect of infill patterns on the mechanical performance of lightweight 3D-printed cellular PLA parts. Materials Today Communications 2018;17:214–28. https://doi.org/10.1016/j.mtcomm.2018.09.017.
[39] Wang AJ, McDowell DL. In-plane stiffness and yield strength of periodic metal honeycombs. Journal of Engineering Materials and Technology, Transactions of the ASME 2004;126:137–56. https://doi.org/10.1115/1.1646165.
[40] Belingardi G, Paolino DS, Koricho EG. Investigation of influence of tab types on tensile strength of E-glass/epoxy fiber reinforced composite materials. Procedia Engineering 2011;10:3279–84. https://doi.org/10.1016/j.proeng.2011.04.541.
[41] Tian X, Liu T, Yang C, Wang Q, Li D. Interface and performance of 3D printed continuous carbon fiber reinforced PLA composites. Compos Appl Sci Manuf 2016;88:198–205. https://doi.org/10.1016/j.compositesa.2016.05.032.
[42] Li N, Li Y, Liu S. Rapid prototyping of continuous carbon fiber reinforced polylactic acid composites by 3D printing. J Mater Process Technol 2016;238:218–25. https://doi.org/10.1016/j.jmatprotec.2016.07.025.
[43] Hao W, Liu Y, Zhou H, Chen H, Fang D. Preparation and characterization of 3D printed continuous carbon fiber reinforced thermosetting composites. Polym Test 2018;65:29–34. https://doi.org/10.1016/j.polymertesting.2017.11.004.
[44] Peng Y, Wu Y, Wang K, Gao G, Ahzi S. Synergistic reinforcement of polyamide-based composites by combination of short and continuous carbon fibers via fused filament fabrication. Compos Struct 2019;207:232–9. https://doi.org/10.1016/j.compstruct.2018.09.014.